Development of Partially-Coherent Wavefront Propagation Simulation Methods for 3rd and 4th Generation Synchrotron Radiation Sources

Oleg Chubar*[a], Lonny Berman[a], Yong S. Chu[a], Andrei Fluerasu[a], Steve Hulbert[a], Mourad Idir[a], Konstantine Kaznatcheev[a], David Shapiro[a], Qun Shen[a], Jana Baltser[b]
[a]Photon Sciences Directorate, Brookhaven National Laboratory, Upton, NY 11973, USA;
[b]Niels Bohr Institute, Copenhagen University, Universitetsparken 5, 2100-Copenhagen Ø, Denmark

ABSTRACT

Partially-coherent wavefront propagation calculations have proven to be feasible and very beneficial in the design of beamlines for 3rd and 4th generation Synchrotron Radiation (SR) sources. These types of calculations use the framework of classical electrodynamics for the description, on the same accuracy level, of the emission by relativistic electrons moving in magnetic fields of accelerators, and the propagation of the emitted radiation wavefronts through beamline optical elements. This enables accurate prediction of performance characteristics for beamlines exploiting high SR brightness and/or high spectral flux. Detailed analysis of radiation degree of coherence, offered by the partially-coherent wavefront propagation method, is of paramount importance for modern storage-ring based SR sources, which, thanks to extremely small sub-nanometer-level electron beam emittances, produce substantial portions of coherent flux in X-ray spectral range. We describe the general approach to partially-coherent SR wavefront propagation simulations and present examples of such simulations performed using "Synchrotron Radiation Workshop" (SRW) code for the parameters of hard X-ray undulator based beamlines at the National Synchrotron Light Source II (NSLS-II), Brookhaven National Laboratory. These examples illustrate general characteristics of partially-coherent undulator radiation beams in low-emittance SR sources, and demonstrate advantages of applying high-accuracy physical-optics simulations to the optimization and performance prediction of X-ray optical beamlines in these new sources.

Keywords: synchrotron radiation, wave optics, partial coherence

1. INTRODUCTION

Over the past decade, many novel experimental techniques relying on X-ray coherence either for scattering or for imaging (e.g. X-ray photon correlation spectroscopy, scanning X-ray microscopy, phase-contrast and coherent diffraction imaging) have emerged. Evidently, traditional beamline ray-tracing analysis has to be extended beyond geometrical optics to include accurate calculation of wave-optical characteristics of SR sources, and to allow for simulation of fully- and partially-coherent SR wavefront propagation through optical elements of a beamline.

After the first wave-optics computer codes for simulation of SR wavefront propagation became available [1 - 4], they have quickly found a number of important practical applications, such as optimization of infrared beamlines in 3rd generation SR sources [5 - 8], simulation and analysis of free-electron laser wavefronts [9 - 11], and electron beam diagnostics [4, 12, 13]. In most of these applications however, simulations were performed only for fully coherent wavefronts.

In the next section, we outline a general (in the framework of the classical electrodynamics) approach to simulation of partially-coherent SR wavefront propagation through optical beamlines of storage rings and Energy-Recovery Linac (ERL) sources. It is essentially based on theoretical works by K.-J. Kim and P. Elleaume [14, 15]. In principle, this approach is also applicable to Free-Electron Lasers (FEL), provided that appropriate numerical description of radiation wavefront at the input of an optical system (i.e. electric field in the case of full coherence, or mutual intensity or brightness in the case of partial coherence approximation) is used. In section 3, we provide results of several numerical simulations illustrating the basic characteristics of partially-coherent Undulator Radiation (UR) in a low-emittance synchrotron source, and make comparisons with predictions of the Gaussian Schell model [16] and a more accurate analytical model proposed in [17] for the UR in 3rd generation sources. All numerical simulations described in this paper were performed using SRW computer code [2 - 4].

*chubar@bnl.gov; phone: 1-631-344-4525

2. THE APPROACH BASICS

Let's first consider spontaneous synchrotron emission by one relativistic electron travelling in magnetic field of an accelerator, and subsequently the emission by an electron beam having given particle distribution in 6D phase space.

2.1 Radiation by One Relativistic Electron

To compute synchrotron radiation emitted by a relativistic electron in free space and observed in the near-field region, an approach based on retarded potentials can be used. With this approach, one can easily obtain the expression for the frequency domain complex electric field of the emitted radiation (Gaussian unit system) [18]:

$$\vec{E}_0 = (ie\omega/c)\int_{-\infty}^{+\infty}[\vec{\beta} - \vec{n}\,[1 + ic/(\omega R)]]\,R^{-1}\exp[i\omega(\tau + R/c)]\,d\tau, \quad (1)$$

where the integration variable τ has dimension of time, ω is cyclic frequency, $\vec{\beta} = \vec{\beta}(\tau)$ is instant relative velocity of the electron (moving e.g. in external magnetic field), $\vec{n} = \vec{n}(\tau)$ is the unit vector directed from instant electron position to an observation point, $R = R(\tau)$ is the distance from the instant electron position to the observation point, c speed of light, e charge of electron.

In the wave zone (at a macro-distance from the electron) it is appropriate to consider only the transverse components of the electric field; besides, we can consider these field components in a transverse plane perpendicular to the "optical axis", before the first optical element of an optical system. These field components depend on transverse coordinates of the observation point x_0, y_0, radiation frequency ω, as well as on initial "coordinates" of electron in 6D phase space (initial horizontal and vertical positions and angles x_e, y_e, x'_e, y'_e, relative energy γ_e and initial longitudinal position z_e): $\vec{E}_{\perp 0} = \vec{E}_{\perp 0}(x_0, y_0, \omega, x_e, y_e, x'_e, y'_e, \gamma_e, z_e)$ The electric field propagation in free space or through an optical element of a beamline can be described by a "propagator", which, for the majority of practically important cases, can be formally represented by:

$$\vec{E}_{\perp j}(x_j, y_j, \omega, x_e, y_e, x'_e, y'_e, \gamma_e, z_e) = \iint \mathbf{K}_j(x_j, y_j, x_{j-1}, y_{j-1}, \omega)\vec{E}_{\perp j-1}(x_{j-1}, y_{j-1}, \omega, x_e, y_e, x'_e, y'_e, \gamma_e, z_e)dx_{j-1}dy_{j-1}, \quad (2)$$

where $\mathbf{K}_j(x_j, y_j, x_{j-1}, y_{j-1}, \omega)$ is a kernel specific to j-th optical element (j = 1, 2, ...), which, in general case, is a matrix (tensor) with its components depending on transverse coordinates in a plane before (x_{j-1}, y_{j-1}) and after (x_j, y_j) the optical element, and frequency; $\vec{E}_{\perp j-1}, \vec{E}_{\perp j}$ are transverse electric fields in the planes before and after the optical element.

For a free space propagation between two parallel planes, following the Huygens-Fresnel principle, in the paraxial approximation this kernel is [19]:

$$\mathbf{K}_j(x_j, y_j, x_{j-1}, y_{j-1}, \omega) \approx \frac{\omega}{2\pi i c L}\exp[i\omega[L^2 + (x_j - x_{j-1})^2 + (y_j - y_{j-1})^2]^{1/2}/c]\,\mathbf{E}, \quad (3)$$

where L is the distance between the planes and $\mathbf{E}$ is the unit matrix; i.e., in this case Eq. (2) is a scalar convolution-type relation for each of the two transverse components of the electric field.

For a "thin" optical element, one can represent the kernel as:

$$\mathbf{K}_j(x_j, y_j, x_{j-1}, y_{j-1}, \omega) \approx \mathbf{T}(x_j, y_j, \omega)\delta(x_{j-1} - x_j)\delta(y_{j-1} - y_j), \quad (4)$$

where $\mathbf{T}(x_j, y_j, \omega)$ is a complex transmission (matrix) function, $\delta(x)$ is delta-function; and Eq. (2) reduces to a product of matrix by vector. For isotropic thin optical element: $\mathbf{T}(x_j, y_j, \omega) = T(x_j, y_j, \omega)\mathbf{E}$, where $T(x_j, y_j, \omega)$ is a scalar complex transmission function. For an optical element with some extent along optical axis, e.g. for a grazing-incidence mirror, one can approximately represent the kernel of Eq. (2) as:

$$\mathbf{K}_j(x_j, y_j, x_{j-1}, y_{j-1}, \omega) \approx \mathbf{G}(x_j, y_j, \omega)\exp[i\omega\Lambda(x_j, y_j, \omega)/c]\delta[x_{j-1} - \tilde{x}_{j-1}(x_j, y_j)]\delta[y_{j-1} - \tilde{y}_{j-1}(x_j, y_j)], \quad (5)$$

where $\mathbf{G}(x_j, y_j, \omega)$ is a matrix function defining local transformations of electric field components (e.g. at reflection from mirror surface), $\tilde{x}_{j-1}(x_j, y_j), \tilde{y}_{j-1}(x_j, y_j)$ are scalar functions defining the transformation of coordinates for points in transverse planes before and after the optical element, $\Lambda(x_j, y_j, \omega)$ is a scalar function defining the corresponding optical path difference. Explicit forms of these functions, or algorithms for their numerical calculation, can be found e.g. by using the stationary phase method, and/or by applying (locally only!) the laws of geometrical optics and boundary conditions for the electric field components.

Within this framework, a numerical simulation of electric field (i.e. wavefront) propagation, from a transverse plane before the first optical element to a plane at a desired location of a beamline, consists in the application of a sequence of "propagators" (see Eqs. (2)), corresponding to the particular optical elements and drift spaces. In many cases, these propagators can have CPU-efficient implementations, e.g. based on Fast Fourier Transforms for convolution-type integrals (see Eqs. (2), (3)) and simple multiplications (see Eqs. (4), (5)). Therefore the entire simulation, even for a wide wavefront containing thousands of transverse coordinates' and frequency values, may take no more than a few seconds on a moderately equipped desktop computer. In the cases of high or full transverse coherence, such as spontaneous infrared emission in 3rd generation sources [5 - 8] (which can be accurately described by Eq. (1)) and FEL emission (with an appropriate input electric field being used instead of Eq. (1)), the entire simulation procedure does not require any other processing, except maybe a straightforward calculation of spectral flux per unit surface (Stokes components) from the propagated electric field components.

However, in storage rings and in ERL, synchrotron emission by entire electron beam is known to be only partially coherent for the most part of spectrum, and more calculations are required for a reliable prediction of its characteristics. In particular, one has to take into account that the radiation is generated by electrons having different initial coordinates, angles and energy, and that the wavefronts produced by these electrons may be propagating differently through optical elements of a beamline. The next sub-section describes how such calculations can be performed in practice.

2.2 Radiation by Electron Beam in Storage Rings and ERL

The flux (number of photons per time unit) per unit surface per unit relative bandwidth of spontaneous radiation by the entire electron beam after propagation through *j*-th optical element of a beamline can be described as:

$$\left(\frac{dN_{ph}}{dtd\Sigma\, d\omega/\omega}\right)_j = \frac{c^2 \alpha\, I_e}{4\pi^2 e^3}\left(I_{ISR\,j} + I_{CSR\,j}\right), \tag{6}$$

where I_e is electron beam current, α is the fine-structure constant; $I_{ISR\,j}$ and $I_{CSR\,j}$ are respectively the contributions of "temporally incoherent" and coherent synchrotron radiation.

The contribution of the "temporally incoherent" radiation, which is dominating in storage ring and ERL sources for the most part of spectrum, can be obtained by averaging the squared amplitude of the electric field from individual electrons over the phase space occupied by the entire electron beam:

$$I_{ISR\,j}(x_j, y_j, \omega) = \int \left|\vec{E}_{\perp j}(x_j, y_j, \omega, x_e, y_e, x'_e, y'_e, \gamma_e, z_e)\right|^2 f(x_e, y_e, x'_e, y'_e, \gamma_e, z_e)\, dx_e dy_e dx'_e dy'_e d\gamma_e dz_e, \tag{7}$$

where the electric field $\vec{E}_{\perp j}$ is obtained from Eq. (1) after application of a sequence of propagators describing optical elements (see Eqs. (2) - (5)). The particle density distribution in 6D phase space is described by the function *f*, which is assumed to be normalized to 1: $\int f(x_e, y_e, x'_e, y'_e, \gamma_e, z_e) dx_e dy_e dx'_e dy'_e d\gamma_e dz_e = 1$. We note that the "temporally- incoherent" SR can have high transverse coherence if the transverse emittance of the electron beam is small.

A simple calculation method for this partially-coherent SR can be based on summing-up of intensities (squared electric field amplitudes) obtained after propagation of the fields from individual "macro-electrons", according to Eqs. (1) - (7). Such simple implementation may appear numerically inefficient for execution on a single-processor computer, however, it can be very easily parallelized for many processors, since electric fields from individual electrons propagate independently. Often, the squared electric field amplitude may not depend on some of the 6D phase space variables (e.g. on z_e), which further simplifies simulations. This method, based on Eqs. (1) - (7), has been used for simulations described in section 3 of this paper.

Accurate calculation of coherent synchrotron radiation contribution, which is usually important only in the far-infrared spectral range in 3rd generation sources, requires less computational resources [20]:

$$I_{CSR\,j}(x_j, y_j, \omega) = \left|\vec{E}_{CSR\perp j}(x_j, y_j, \omega)\right|^2, \tag{8}$$

where $\vec{E}_{CSR\perp j}$ is a sum of electric fields from all electrons, which can be originally calculated before first optical element:

$$\vec{E}_{CSR\perp 0}(x_j, y_j, \omega) \approx N_e^{1/2} \int \vec{E}_{\perp 0}(x_j, y_j, \omega, x_e, y_e, x'_e, y'_e, \gamma_e, z_e) f(x_e, y_e, x'_e, y'_e, \gamma_e, z_e) dx_e dy_e dx'_e dy'_e d\gamma_e dz_e, \tag{9}$$

and then propagated through optical elements, using the same propagators as for the electric fields from individual electrons:

$$\vec{E}_{CSR\perp j}(x_j, y_j, \omega) = \iint \mathbf{K}_j(x_j, y_j, x_{j-1}, y_{j-1}, \omega) \vec{E}_{CSR\perp j-1}(x_{j-1}, y_{j-1}, \omega) dx_{j-1} dy_{j-1}. \tag{10}$$

N_e in Eq. (9) is the number of electrons in a bunch (we note that I_e in Eq. (6) is proportional to N_e, so the "temporally incoherent" contribution to the spectral flux is proportional to N_e, whereas that of the coherent SR to N_e^2).

The propagation of partially-coherent synchrotron radiation can also be described in terms of mutual intensity [19]:

$$M_j = M_{ISR\,j} + M_{CSR\,j}, \tag{11}$$

$$\begin{aligned} M_{ISR\,j}(x_j, y_j, \omega, \tilde{x}_j, \tilde{y}_j, \tilde{\omega}) = \int \vec{E}_{\perp j}(x_j, y_j, \omega, x_e, y_e, x'_e, y'_e, \gamma_e, z_e) \vec{E}^*_{\perp j}(\tilde{x}_j, \tilde{y}_j, \tilde{\omega}, x_e, y_e, x'_e, y'_e, \gamma_e, z_e) \times \\ \times f(x_e, y_e, x'_e, y'_e, \gamma_e, z_e) dx_e dy_e dx'_e dy'_e d\gamma_e dz_e, \end{aligned} \tag{12}$$

$$M_{CSR\,j}(x_j, y_j, \omega, \tilde{x}_j, \tilde{y}_j, \tilde{\omega}) = \vec{E}_{CSR\perp j}(x_j, y_j, \omega) \vec{E}^*_{CSR\perp j}(\tilde{x}_j, \tilde{y}_j, \tilde{\omega}), \tag{13}$$

where "*" means complex conjugation. $I_{ISR\,j}$ and $I_{CSR\,j}$ (see Eq. (6)) can be considered as the corresponding mutual intensities taken at $\tilde{x}_j = x_j, \tilde{y}_j = y_j, \tilde{\omega} = \omega$.

Optical element propagators for mutual intensity can be obtained from the corresponding propagators for the electric field (see Eq. (2) - (5)); and so in terms of the mutual intensity, partially-coherent wavefront propagation can be simulated as "one pass" through the sequence of individual optical element propagators describing a beamline, similarly to how this is done for the electric field in the case of a fully-coherent wavefront. However, as different from the electric field, which depends only on two transverse coordinates and frequency, mutual intensity depends on four coordinates (direct x_j, y_j and "conjugate" $\tilde{x}_j, \tilde{y}_j$ ones) and two frequencies ($\tilde{\omega}, \omega$). Numerical manipulation with such a 6-dimentional entity, and even just tabulating and storing it in active memory of a computer may represent a serious practical problem. Nevertheless, in those cases when wavefront sampling doesn't need to be very dense, or for wavefronts which effectively depend on one transverse coordinate, the partially-coherent wavefront propagation simulation based on the mutual intensity may represent a well affordable task of high practical interest.

Another reason for which one may be interested in using the mutual intensity is that it is linked by Fourier transformation to the mathematical brightness (or Wigner distribution), which can be considered as phase-space distribution function of a photon beam [14, 15]:

$$B_j(x_j, y_j, x'_j, y'_j, \omega, t) \sim \omega^2 \int_{-\infty}^{+\infty} \int_{-\infty}^{+\infty} \int_{-\infty}^{+\infty} M_j(x_j, y_j, \omega, \tilde{x}_j, \tilde{y}_j, \tilde{\omega}) \exp[-i\omega(x'\tilde{x} + y'\tilde{y})/c - i\tilde{\omega}t] d\tilde{x} d\tilde{y} d\tilde{\omega} \tag{14}$$

Even though mathematical brightness is not a positively-defined function, and can obtain negative values for some types of distributions (e.g. for even harmonics of UR [15]), for Gaussian-like radiation sources, the mathematical brightness calculated for a longitudinal position of the source is one of the most important practical characteristics [14, 15, 21, 22].

3. EXAMPLES OF NUMERICAL SIMULATIONS

3.1 Apparent Angular Divergences and "Source Sizes" of a Partially-Coherent Undulator Radiation Beam

For a large number of beamline design tasks, accurate values of the horizontal and vertical angular divergences and the "source sizes" of UR beam are necessary. These values have to include contributions of angular divergences and diffraction-limited source sizes of single-electron UR, as well as the divergences and sizes of the finite-emittance electron beam. Even though approximate values of the divergences and source sizes can be obtained by analytical formulae [21, 22], more accurate values may require numerical partially-coherent wavefront propagation calculations. An example of such calculations, performed for two slightly different photon energy values at 5th harmonic of the radiation from a 20 mm period, 3 m long hybrid in-vacuum undulator of NSLS-II, is presented in figure 1. One of the photon energy values used (10.009 keV) is exactly the on-axis resonant photon energy of the single-electron UR, whereas the other value (9.996 keV) was chosen to be closer to the peak of the UR spectral flux collected through a 100 μrad (h) x 50 μrad (v) angular aperture, which is comparable to a typical angular acceptance of a hard X-ray beamline in a 3rd generation source (figure 1-a).

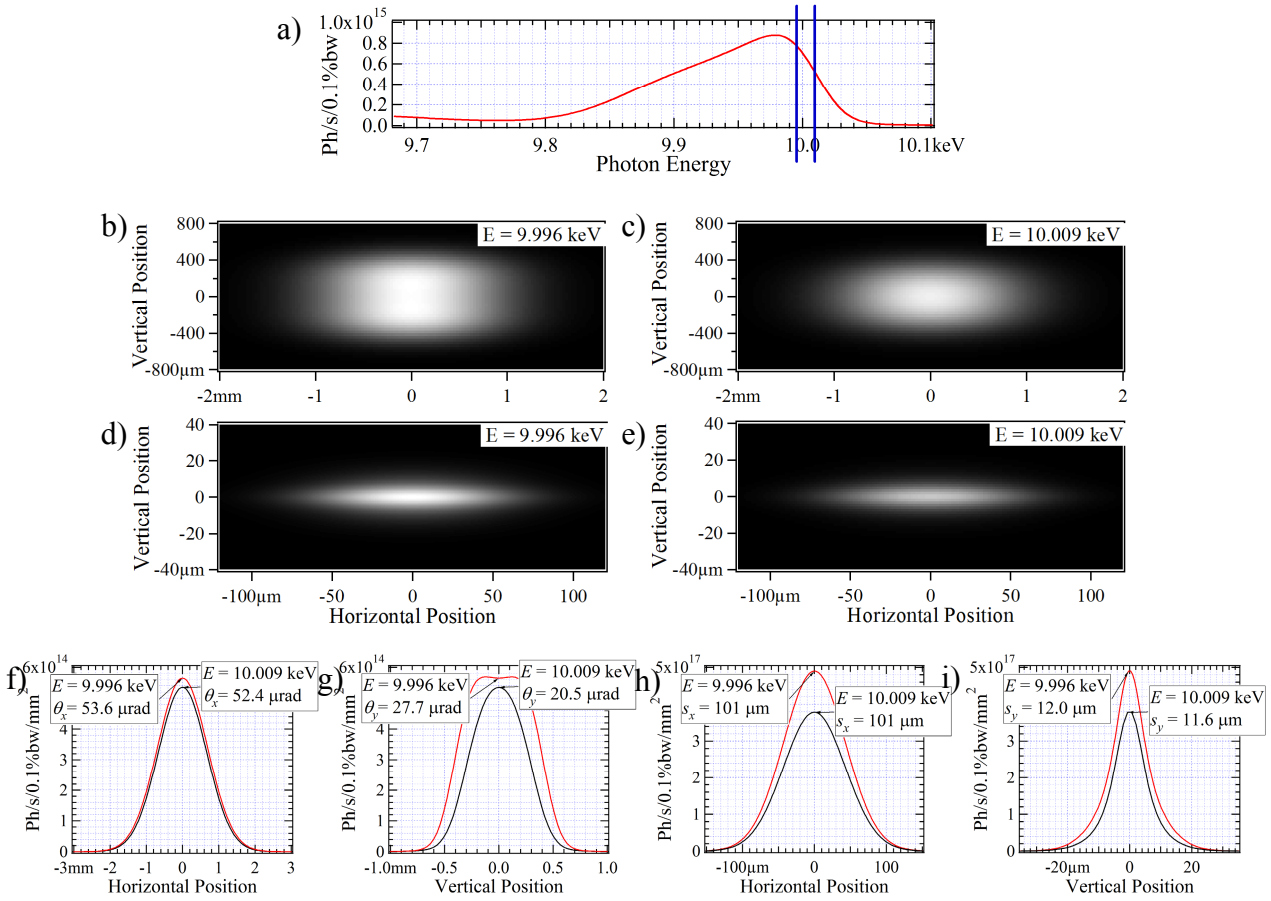

Figure 1. Spectral flux and intensity distributions of radiation from 20 mm period 3 m long in-vacuum undulator of NSLS-II, tuned to have 5th harmonic at ~10 keV: a) spectral flux collected through 100 μrad (hor.) x 50 μrad (vert.) angular aperture; b, c) intensity distributions at 30 m from the undulator at 9.996 keV photon energy (shown by left vertical line in (a)) and at 10.009 keV photon energy (shown by right line in (a)); d, e) intensity distributions in the 1:1 image plane; f, h) horizontal cuts of intensity distributions at 30 m from the undulator (f) and in the 1:1 image plane (h); g, i) vertical cuts of intensity distributions at 30 m from the undulator (g) and in the 1:1 image plane (i).

To estimate the X-ray beam angular divergences at these two photon energies, we calculated the corresponding UR intensity distribution for an observation plane located relatively far (at 30 m) from the undulator (figures 1-b,c). Then, in order to estimate the apparent X-ray beam source sizes, we considered a simple 1:1 focusing scheme consisting of one ideal lens, and calculated, using the partially-coherent wavefront propagation method, intensity distributions in the image plane of this scheme, i.e. at 60 m from the undulator (figures 1-d,e). For these calculations, the "day 1" horizontal and vertical emittances and energy spread of the electron beam (0.9 nm, 8 pm and 8.9×10^{-4} respectively), and the nominal horizontal and vertical beta-function values of NSLS-II low-beta straight section (2.02 m and 1.06 m respectively) were used. The FWHM values of the horizontal and vertical angular divergences (θ_x, θ_y) and source sizes (s_x, s_y), obtained from these calculations, are given in figures 1-f,g,h,i.

In addition to the observation that the maximal UR flux from a finite-emittance electron beam collected through a finite aperture doesn't correspond to the on-axis resonant photon energy of single-electron UR [15], we note that in the vertical plane, the multi-electron UR intensity distributions both at a distance from the undulator (figures 1-b,c,g), and in the 1:1 image plane (figures 1-d,e,i) differ from Gaussian, especially for photon energies not equal to the on-axis resonant energy of a single-electron UR harmonic.

It can be useful to estimate apparent "phase-space volume" occupied by this partially-coherent UR beam and to compare it to the well-known values for the fully-coherent Gaussian beam at the same wavelength ($\lambda/4\pi$). Such comparisons, performed both for RMS ($\sigma_{ph}, \sigma'_{ph}$) and FWHM ($s_{ph}, s'_{ph}$) values of the corresponding intensity distributions, are presented in table 1. In the second column of table 1, ratios of the horizontal and vertical electron beam emittance (ε_e) to the phase-space volume of a fully-coherent Gaussian beam at ~10 keV photon energy are given. We see that in the horizontal plane, the phase-space volume of the resulting photon beam is dominated by the volume occupied by the electron beam. On the other hand, in the vertical plane, the electron beam emittance is small, and the additional phase-space volume of the resulting photon beam (compared to that of the coherent Gaussian beam), is explained by deviation of the single-electron UR distribution from Gaussian, and by contribution of the electron beam energy spread to the UR angular divergence and source size [22].

From the phase-space volumes presented in table 1 and the spectral flux shown in figure 1-a, one can estimate the apparent brightness and the "transversely coherent flux" [14, 21] portion of the partially-coherent UR source. For the resonant photon energy (10.009 keV), the estimated apparent brightness is $\sim 2.9 \times 10^{20}$ ph/s/.1%bw/mrad^2/mm^2 and the coherent flux $\sim 1.1 \times 10^{12}$ ph/s/.1%bw (which represents $\sim 2 \times 10^{-3}$ fraction of the total flux emitted at that photon energy); for the "red-shifted" photon energy (9.996 keV) the apparent brightness and the coherent flux values are, respectively, $\sim 3.3 \times 10^{20}$ ph/s/.1%bw/mrad^2/mm^2 and $\sim 1.3 \times 10^{12}$ ph/s/.1%bw (the latter value representing $\sim 1.6 \times 10^{-3}$ fraction of the corresponding total flux). Results of detailed partially-coherent wavefront propagation simulations performed for the Hard X-ray Nanoprobe beamline of NSLS-II, which will be operating at the above parameters of electron beam and undulator, were published in [23, 24].

Table 1. Comparison of the apparent phase-space volume occupied by a partially-coherent UR beam at ~10 keV photon energy (at the 5th undulator harmonic) to that of a fully-coherent Gaussian beam, for the case of 0.9 nm (8 pm) horizontal (vertical) emittance and 8.9×10^{-4} relative energy spread of a 3 GeV electron beam.

Phase-space volume ratios:	$\varepsilon_e \cdot 4\pi/\lambda$	$\sigma_{ph}\sigma'_{ph} \cdot 4\pi/\lambda$		$[s_{ph}s'_{ph}/(2.35)^2] \cdot 4\pi/\lambda$	
		$\lambda = \lambda_n$	$\lambda \approx 1.0013\lambda_n$*	$\lambda = \lambda_n$	$\lambda \approx 1.0013\lambda_n$*
Horizontal plane	91.2	97.3	99.5	97.2	99.3
Vertical plane	0.81	~5.1**	~6.5**	4.4	6.1

* In terms of harmonic number (n = 5), number of undulator periods (N = 150) and on-axis resonant wavelength of the harmonic ($\lambda_n \approx 1.2387$ Å), this wavelength value is: $\lambda \approx (1 + 0.97/(nN))\lambda_n$

** The RMS values for the vertical plane were calculated for the portions of intensity distributions containing ~99% of total flux.

3.2 Degree of Coherence of Undulator Radiation in 3rd Generation Synchrotron Radiation Sources

Estimation of the degree of coherence of undulator radiation in 3rd generation sources represents a topic of high practical importance, which was considered in [16, 17] and in other works. In [16], the use of the Gaussian Schell model

for the analytical description of partially-coherent UR has been proposed, which was a step forward compared to direct application of the standard Van Cittert - Zernike theorem [19] to these highly anisotropic radiation sources. More detailed theoretical analysis of partially-coherent UR revealed deviation of the degree of transverse coherence predicted by the Gaussian Schell model from the values resulting from a more accurate theoretical treatment taking into account non-Gaussian shape of single-electron UR distribution and large difference between horizontal and vertical electron beam emittances in 3rd generation sources [17].

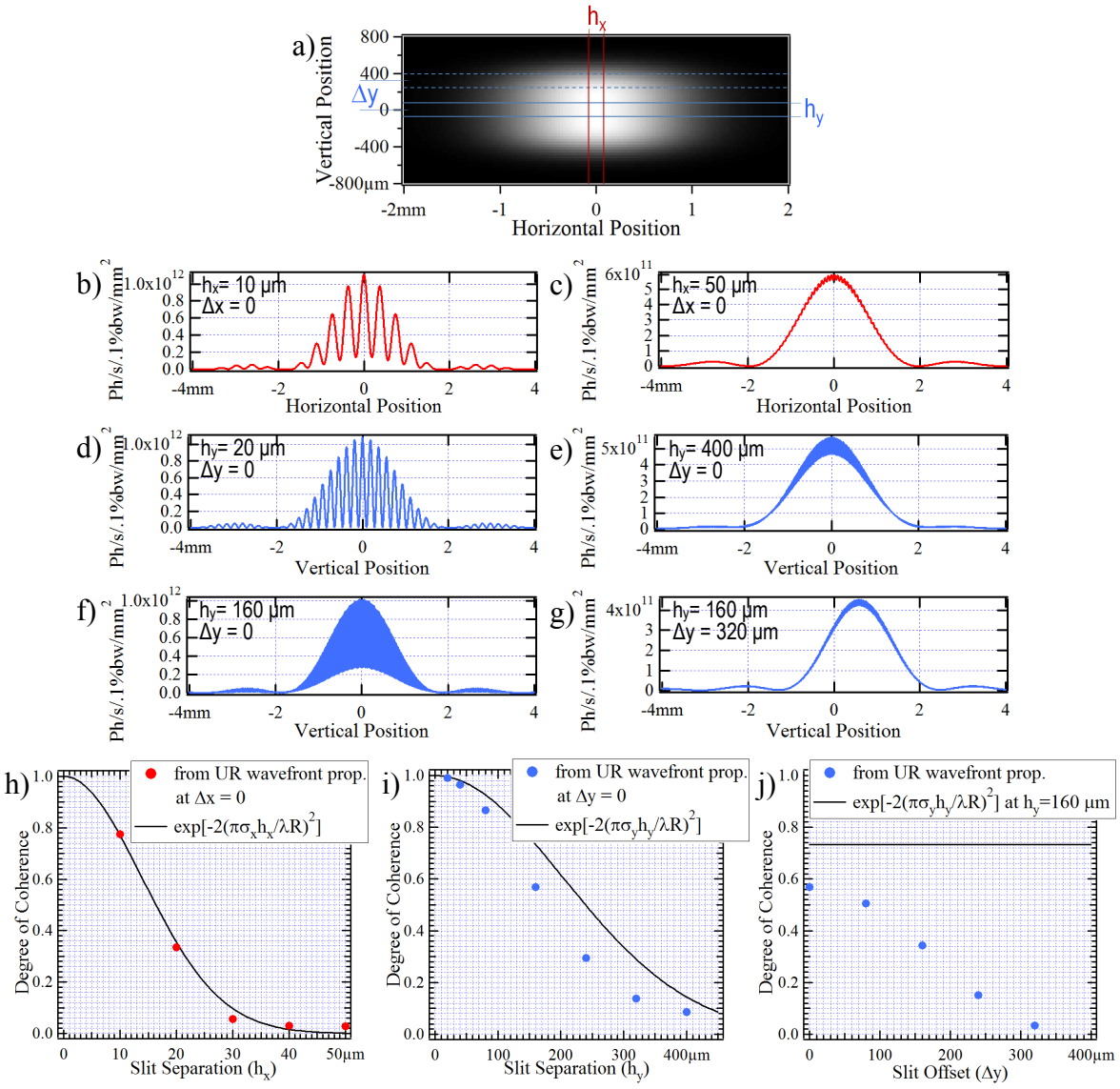

Figure 2. a) UR intensity distribution at ~10 keV photon energy (5th harmonic) used for the analysis of the degree of coherence (slits are shown by lines); b, c) horizontal cuts of the interference patterns calculated for two different separations of the vertical slits, without horizontal offset of the slits from symmetrical positions; d, e) vertical cuts of the interference patterns calculated for two different separations of the horizontal slits, without vertical offset of the slits from symmetrical positions; f, g) vertical cuts of the interference patterns calculated for a fixed separation of the horizontal slits, with and without vertical offset of the slits from symmetrical positions; h, i, j) comparison of the numerically estimated degree of transverse coherence of undulator radiation with the predictions of the Gaussian Schell model, in the horizontal (h) and vertical (i, j) directions (λ is the radiation wavelength and R is the distance from the undulator to the slits).

To verify numerically the theoretical predictions [17], we have considered Young's two-slit interference schemes with (2 μm wide) horizontal and vertical slits located at R = 30 m distance from the center of undulator, and calculated the intensity distributions of interfering UR at 30 m distance from the slits. The UR parameters were exactly the same as in the previous numerical example (the radiation at 9.996 keV photon energy at 5th harmonic of UR spectrum was used; the spectral flux vs photon energy at this harmonic is shown in figure 1-a). We analyzed the visibility of fringes at different horizontal and/or vertical separation (h_x, h_y) between the two slits positioned symmetrically with respect to center of the UR intensity distribution, and at different vertical offset of the two horizontal slits from this symmetrical position (Δy), see figure 2-a. Figures 2-b,c show horizontal cuts of intensity distribution calculated for two different separations of the vertical slits: h_x= 10 μm and 50 μm, without any horizontal offset of the slits from the symmetrical position (Δx = 0). As expected, one observes a considerably higher visibility of fringes at h_x= 10 μm. The obtained dependence of the degree of coherence (equal to the visibility of fringes for the symmetrical location of the slits) on the separation between the slits agrees well with the prediction of the Gaussian Schell model for the horizontal direction (figure 2-h). However, similar estimations performed for the vertical direction, i.e. for the horizontal slits located symmetrically (Δy = 0) at vertical separation h_y varying from 20 μm to 400 μm (figures 2-d,e,i) differ from the Gaussian model predictions (see figure 2-i). We note that at these comparisons, the following values of the horizontal and vertical RMS electron beam sizes were used: $\sigma_x \approx$ 43 μm, $\sigma_y \approx$ 2.9 μm.

Next, we consider variation of the visibility of fringes and the corresponding degree of coherence with a vertical offset of the horizontal slits (Δy), at constant vertical separation between them (h_y= 160 μm), see figures 2-f,g,j. We note that for non-equal intensities within the slits ($I_1 \neq I_2$), the degree of coherence g_{12} is formally related to the visibility of fringes V as [19]:

$$g_{12} = V \cdot (I_1 + I_2)/[2(I_1 I_2)^{1/2}] \tag{15}$$

However, in our case, even for the maximal considered offset of the slits (Δy = 320 μm), g_{12} and V differ, according to Eq. (15), by no more than ~5%. On the other hand, as one can see from figure 2-j, the deviation (decrease) of the degree of coherence from the Gaussian Schell model prediction at the considered UR parameters is very significant, in agreement with [17]. This effect can be explained by special features of the coherent single-electron UR [25]. One can note that a similar effect (i.e. increase of the effective incoherent source size at the observation off the emission axis) is known to take place also in the case of wiggler radiation [26]. These features of the undulator and wiggler radiation in 3rd generation SR sources have to be taken into account at the optimization of beamlines for experiments requiring X-ray coherence.

4. CONCLUSIONS

We described a high-accuracy physical-optics based approach for the simulation of partially-coherent synchrotron radiation wavefront propagation in beamlines of 3rd and 4th generation sources, and presented examples of such simulations, illustrating the basic characteristics of the undulator radiation in a low-emittance synchrotron source. Deviations of these characteristics from the predictions of the Gaussian Schell model were discussed. The described approach has a large number of potential applications of high importance for the design of new SR beamlines, optical metrology, source and optical element diagnostics, and for experiments exploiting high coherence and brightness of synchrotron radiation offered by new sources. The theory of this approach, which covers, in the same framework of classical electrodynamics, both the processes of the emission and propagation of fully- and partially-coherent synchrotron radiation wavefronts, is known, and implementations of the elements of this theory in computer codes exist [1 - 4]. However, a lot of work has yet to be done to increase generality, numerical efficiency and reliability of the computer codes, as well as to improve interfaces to allow for the use of these codes by larger numbers of scientists and engineers working on storage rings, ERL, FEL and laboratory sources.

ACKNOWLEDGEMENTS

The idea of the "Synchrotron Radiation Workshop" computer code, which has been extensively used for simulations presented in this paper, belongs to Pascal Elleaume (ESRF).

Authors are grateful to G. Geloni, L. Samoylova (European XFEL), E. Saldin (DESY), A. Snigirev (ESRF), R. Reininger, V. De Andrade, K. Evans-Lutterodt, L. Wiegart, P. Ilinski and H. Yan (BNL) for collaboration and fruitful discussions.

Work is supported by US DOE, Contract No. DE-AC02-98CH10886.

REFERENCES

[1] Bahrdt, J., “Wavefront propagation: design code for synchrotron radiation beamlines”, Applied Optics 36 (19), p.4367 (1997).
[2] Chubar, O. and Elleaume, P., "Accurate and efficient computation of synchrotron radiation in the near field region", Proc. EPAC-98, 1177-1179 (1998).
[3] Chubar, O., “Wavefront calculations”, Proc. SPIE 4143, 48-60 (2000).
[4] Chubar, O., Elleaume, P., Kuznetsov, S. and Snigirev, A., "Physical optics computer code optimized for synchrotron radiation", Proc. SPIE 4769, 145-151 (2002).
[5] Reininger, R. and May, T., "Wave propagation through the far infrared beamline at the CLS", Proc. SRI-2003, AIP Conf. Proc. vol. 705, 462 - 465 (2004).
[6] Dumas, P., Polack, F., Lagarde, B., Chubar, O., Giorgetta, J.L. and Lefrancois, S., “Synchrotron infrared microscopy at the French synchrotron facility SOLEIL”, Infrared Physics & Technology 49, 152-160 (2006).
[7] Roy, P., Rouzieres, M., Qi, Z., Chubar,O., “The AILES infrared beamline on the third generation synchrotron radiation facility SOLEIL”, Infrared Physics & Technology 49, 139-146 (2006).
[8] Chubar, O., Susini, J., Cotte, M., Polack, F., Lagarde, B., Scheidt, K., Elleaume, P. and Dumas, P., “Simulation and optimization of synchrotron infrared micro-spectroscopic beamlines using wave optics computation: ESRF and SOLEIL cases”, Proc. SRI-2006, AIP Conf. Proc. vol. 879, 607-610 (2007).
[9] Reininger, R., Feldhaus, J., Gürtler, P. and Bahrdt, J., "Wavefront propagation through the beamline designed for seeding the DESY XUV FEL", Nucl. Instrum. and Meth. A 467, 38 (2001).
[10] Bahrdt, J., "Wavefront tracking within the stationary phase approximation", Phys. Rev. ST - Accel. Beams 10 (2007) 060701.
[11] Chubar, O., Couprie, M.-E., Labat, M., Lambert, G., Polack, F., Tcherbakoff, O., “Time-dependent FEL wavefront propagation calculations: Fourier optics approach”, Nucl. Instr. and Meth. A 593, 30-34 (2008).
[12] Chubar, O., Snigirev, A., Kuznetsov, S., Weitkamp, T., Kohn, V., “X-ray interference methods of electron beam diagnostics”, Proc. DIPAC-2001, 88-90 (2001).
[13] Tordeux, M.-A., Cassinari, L., Chubar, O., Denard, J.-C., Pedeau, D., Pottin, B., "Ultimate resolution of SOLEIL X-ray pinhole camera", Proc. DIPAC-2007, 180-182 (2007).
[14] Kim, K.-J., "Brightness, coherence and propagation characteristics of synchrotron radiation", Nucl. Instr. and Meth. A 246, 71-76 (1986).
[15] Elleaume, P., "Generalities on the synchrotron radiation" and "Undulator radiation", in "Undulators, wigglers and their applications", ed. by Onuki, H. and Elleaume, P., Taylor and Francis, London, 38-107 (2003).
[16] Coisson, R., Marchesini, S., "Spatial coherence of synchrotron radiation", Applied Optics 34, No. 5, 904-908 (1995).
[17] Geloni, G., Saldin, E., Schneidmiller, E. and Yurkov, M., "Transverse coherence properties of X-ray beams in third-generation synchrotron radiation sources", Nucl. Instr. and Meth. A 588, 463-493 (2008).
[18] Chubar, O., “Precise computation of electron beam radiation in non-uniform magnetic fields as a tool for the beam diagnostics”, Rev. Sci. Instrum. 66(2), 1872-1876 (1995).
[19] Born, M., Wolf, E., Principles of Optics, 7th ed., Cambridge University, Cambridge (1999).
[20] Chubar, O., “Simulation of emission and propagation of coherent synchrotron radiation wave fronts using the methods of wave optics”, Infrared Physics & Technology, 49, 96-103 (2006).
[21] Kim, K.-J., "Characteristics of synchrotron radiation", in X-Ray Data Booklet, 2nd ed., LBNL, Univ. of California, Berkeley (2001).

[22] Tanaka, T. and Kitamura, H., "Universal function for the brilliance of undulator radiation considering the energy spread effect", J. Synchrotron Rad., 16, 380-386 (2009).
[23] Chubar, O., Chu, Y. S., Kaznatcheev, K. and Yan, H., "Performance optimization for hard X-ray microscopy beamlines guided by partially-coherent wavefront propagation calculations", Proc. SRI-2009, AIP Conf. Proc. vol. 1234, 185-188 (2010).
[24] Chubar, O., Chu, Y. S., Kaznatcheev, K. and Yan, H., "Application of partially coherent wavefront propagation calculations for design of coherence-preserving synchrotron radiation beamlines", Nucl. Instr. and Meth. A 649, 118-122 (2011).
[25] Chubar, O., Elleaume, P. and Snigirev, A., “Phase analysis and focusing of synchrotron radiation”, Nucl. Instr. and Meth. A 435, 495-508 (1999).
[26] Walker, R.P., "Bending magnet and wiggler radiation", in "Undulators, wigglers and their applications", ed. by Onuki, H. and Elleaume, P., Taylor and Francis, London, 108-147 (2003).